Supplementary Information

Enhancing the inherent catalytic activity and stability of TiO_2 supported Pt single-atoms at CeO_x–TiO_2 interfaces

Mi Yoo [a,‡], Eunji Kang [a,‡], Hyuk Choi [a,‡], Hyunwoo Ha[a], Hanseul Choi[b,c], Jin-Seok Choi[d], Kug-Seung Lee[e], Richard Celestre[f], David A. Shapiro[f], Jeong Young Park[b,c,*], Chunjoong Kim[a,*], Young-Sang Yu[f,g,*] and Hyun You Kim[a,*]

[a]Department of Materials Science and Engineering, Chungnam National University, Daejeon 34134, Republic of Korea.

[b]Center for Nanomaterials and Chemical Reactions, Institute for Basic Science (IBS), Daejeon 34141, Republic of Korea

[c]Department of Chemistry, Korea Advanced Institute of Science and Technology (KAIST), Daejeon 34141, Republic of Korea

[d]KAIST Analysis center for Research Advancement, Korea Advanced Institute of Science and Technology (KAIST), Daejeon 34141, Republic of Korea

[e]Pohang Accelerator Laboratory, Pohang University of Science and Technology, Pohang 37673, Republic of Korea

[f]Advanced Light Source, Lawrence Berkeley National Laboratory, Berkeley, California 94720, United States of America.

[g]Advanced Light Source, Lawrence Berkeley National Laboratory, Berkeley, California 94720, United States of America.

‡These authors contributed equally to this work

*To whom correspondence should be addressed: Prof. Young-Sang Yu (youngsang@chungbuk.ac.kr), Prof. Jeong Young Park (jeongypark@kaist.ac.kr), Prof. Chunjoong Kim (ckim0218@cnu.ac.kr), and Prof. Hyun You Kim (kimhy@cnu.ac.kr)

Contents

1. Methods

Synthesis of *n*PT and *n*PCT Catalysts

All catalysts were synthesized by wet impregnation method[1]. Titanium (IV) oxide (anatase, #45603, Alfa Aesar) powder and cerium (III) nitrate hexahydrate ($CeN_3O_9 \cdot 6H_2O$, #11330, Alfa Aesar) powder were used to prepare the CeO_x-TiO_2 supporting oxide powders; chloroplatinic acid (H_2PtCl_8 8 wt.% in H_2O, Sigma-Aldrich) solution was used as the metal precursor. As-received anatase-TiO_2 powders were heat-treated under air at 500 °C for 4 hours before use.

To synthesize CeO_x-TiO_2 supporting oxide, TiO_2 powder (1 g) and Ce precursor (0.019 g, 1wt.%) were dispersed in 60 ml of deionized (DI) water and stirred for 2 hours at 70 °C. The solution was dried at 110 °C for 12 hours and calcined in air at 500 °C for 8 hours with a heating rate of 2 °C·min^{-1}. For the preparation of *n*PT and *n*PCT catalysts, the varying amounts of Pt precursors were added to 60 mL of deionized water with 1 g of CeO_x-TiO_2 or TiO_2 powder. To intensively study the intrinsic catalytic performance of Pt-SAs, the initial amount of Pt was set to 0.05, 0.10, and 0.25 wt.% with respect to the total weight of *n*PT or *n*PCT catalysts. After Pt impregnation, the particles were dried at 110 °C for 12 hours and calcined in air at 500 °C for 3 hours to remove the residual chlorine.

High-Angle Annular Dark-Field Scanning Transmission Electron Microscopy

Images of Pt species dispersed on TiO_2 and CeO_x-TiO_2 supports were acquired by high-angle annular dark-field (HAADF) scanning transmission electron microscopy (STEM) analysis using Titan Double CS-corrected TEM (Titan cubed G2 60-300, FEI). The microscope was operated at an accelerating voltage in the range of 60 to 300 kV. Samples were prepared by drop-casting a dilute nanoparticle solution on a carbon-coated copper grid with lacey carbon film.

X-ray Photoelectron Spectroscopy

X-ray photoelectron spectroscopy (XPS) spectra were collected with a K-Alpha+ system (Thermo Fisher Scientific) to characterize the oxidation state of individual ions of CeO_x-TiO_2 oxide supports and *n*PT and *n*PCT catalysts. Binding energies were estimated using

the C 1*s* signal at 284.8 eV as a reference. Quantitative analysis was carried out using the peak area obtained considering the chemical state identified from the exact peak position[2,3].

Pt-L_3 X-ray Absorption Spectroscopy

Pt-L_3 X-ray absorption spectroscopy (XAS) analysis was performed on the catalysts across the Pt L_3-edge using the 8C beamline at Pohang Accelerator Laboratory (PAL) with a Si (111) double-crystal monochromator. The raw spectra of all samples were energy-calibrated with a Pt foil in front of the third ion chamber simultaneously, and the spectra were acquired in transmission mode using a gas ionizing detector at room temperature. The raw data was normalized using SIXpack[4]. Detailed structural refinement using XAFS was not studied in this work due to complexity of the structure in the nanoscale. XANES spectra were fitted by a linear combination using reference standard spectra of Pt and PtO_2 to provide quantitative information about degree of oxidation of Pt among the catalysts (Table S2). The quality of each linear-combination fit was checked with the *R*-factor defined as, $R = \sum(\text{data - fit})^2 / \sum(\text{data})^2$.

***Operando* gas X-ray Absorption Spectroscopy and Scanning Transmission X-ray Microscopy Analysis**

Operando gas X-ray absorption spectroscopy (XAS) and scanning transmission X-ray microscopy (STXM) analysis were carried out at the elliptically polarizing undulator beamline (7.0.1.2) at the Advanced Light Source (ALS), Lawrence Berkeley National Laboratory, Berkeley, CA (USA)[5]. The catalytic particles were sealed in a microfluidic heating cell (Hummingbird Scientific 1300 series) designed for environmental transmission electron microscope (ETEM)[1,6,7]. The microfluidic heating cell consists 50-nm-thick SiN_x membrane sandwich separated by a spacer with thickness of 2 μm gap for gas flow. The temperature of the micro-heater was controlled *via* the temperature-dependent resistivity with a closed-loop control. The resistivity versus temperature dependency of the heater was calibrated by the manufacturer (Hummingbird Scientific) on each batch of fabricated chips. To verify the reaction mechanism and stability of the catalyst under actual reaction conditions, a blend of Ar with 1 vol% CO and 4 vol% O_2 was flowed into the heating cell through a 300 cm long polyether ether ketone (PEEK) tube at a flow rate of 3 sccm. The Ce *M*-edge spectrum of the

catalyst particles sealed in the heating cell was collected during the process of increasing the temperature from room temperature to 300°C and maintaining it at 300°C for 14 hours. Also, the same process under 100% Ar was performed to accurately compare the effect of the reaction gas condition.

Image Processing

To eliminate image-to-image wobble with sub-pixel precision, the geometric transformation matrix between sequential STXM images was calculated by the intensity-based image registration (MathWorks, MATLAB R2019a) and applied to each image with bilinear interpolation. The transmitted intensity images were converted to the absorbance image spectra (optical density, OD) by following Beer-Lambert law. In the averaged STXM image across the energy range, the pixels of which transmitted intensity were in top 95 % were considered as a sample-free region for estimating I_0. To enhance the signal-to-noise ratio, the image spectra were filtered by local-means. The quantitative distributions of distinct chemical phases were mapped by analyzing the image spectra on a pixel-by-pixel basis with the linear superposition of the reference spectra (Fig. S10). The relative amounts of each component were calculated by applying non-negative least squares. The quality of each linear-combination fit was checked with the *R*-factor defined as, $R = \sum(\text{data - fit})^2 / \sum(\text{data})^2$. Pixels showing poor signal-to-noise ratios were filtered out by a lower bound of the *R*-factor (0.5).

Catalytic Characterization

The catalytic performance of *n*PT and *n*PCT catalysts for CO oxidation was measured in a fixed-bed quartz flow microreactor. For CO oxidation reaction, we used 100 mg of catalyst mixed with 200 mg of quartz sand and loaded on the quartz wool to prevent displacement of the catalyst. The reaction gas consisted of 1 vol% CO, 4 vol% O_2, and 95 vol% Ar and was fed at 50 mL·min^{-1}, corresponding to a weight hourly space velocity (WHSV) of 60,000 mL·g^{-1}·h^{-1}. The light-off curve was measured with a ramping rate at 3 °C·min^{-1}, after activating the catalysts in the reaction atmosphere up to 300 °C. The CO conversion ratio (%) was defined as $100 \times (\text{mol CO}_{,\text{in}} - \text{mol CO}_{,\text{out}})/\text{mol CO}_{,\text{in}}$. The signal of CO was corrected for the contribution from the cracking fragment of CO_2 with mass concentration determination mode. Activation energy barriers (E_{act}) were calculated for CO oxidation below 10% conversion. The order of

reaction values with CO of the catalysts were determined by collecting the reaction rate of the catalysts by increasing the partial pressure of CO from 0.01 bar to 0.05 bar under the fixed O_2 partial pressure of 0.01 bar at T_{10} (10% CO conversion). The turnover frequencies (TOFs) were calculated using the number of CO_2 molecules formed per second divided by the number of Pt atoms deposited on the CeO_x-TiO_2 and TiO_2 surface. 100 mg of a 0.05PT and 0.05PCT used for a CO oxidation contain ~1.54×10^{17} Pt atoms (Table S3)

CO-temperature programmed reaction (CO-TPR) tests were performed to verify the operation of the Mars-van Krevelen mechanism on 0.05PT and 0.05PCT catalysts including CeO_x-TiO_2 and TiO_2 powders. Samples were pretreated at 300 °C for an hour under Ar 100 vol % after repeating two cycles of CO oxidation reaction for pre-activation. We used 100 mg of catalyst mixed with 200 mg of quartz sand and loaded on the quartz wool. The reaction gas consisted of 1 vol% CO and 99 vol% Ar and was fed at 100 $mL \cdot min^{-1}$, corresponding to a weight hourly space velocity (WHSV) of 60,000 $mL \cdot g^{-1} \cdot h^{-1}$. A ramping rate of 1 $°C \cdot min^{-1}$ applied from 50 °C to 300 °C and the catalyst was maintained at 300 °C for 4 hours. The CO_2 concentration in the outlet gas was measured *in-situ*.

The long-term catalytic stability of 0.05PT and 0.05PCT was tested by proceeding a continuous CO oxidation reaction at 300 °C. After initial three hysteric CO oxidation test cycles, the catalyst was immediately exposed to the CO oxidation condition at 300 °C for 12~24 hours and cooled down to 50 °C under 4 vol% O_2 and 96 vol% Ar flow. The final light-off curve after the long-term test was acquired from the subsequent heating process. Refer to **Fig. S7a** for schematic time-temperature profile.

All of the above measurements were performed in a fixed-bed quartz flow microreactor and monitored in real time with a quadrupole mass spectrometer (QMS, PFEIFFER Vacuum GSD320) connected to the reactor outlet.

In situ Diffuse Reflectance Infrared Fourier Transform Spectroscopy Analysis

In situ DRIFTS spectra were obtained by a Fourier-transform infrared spectrometer (Agilent, Cary 660) with a mercury cadmium telluride detector. About 3 mg of sample was pressed onto stainless mesh. Each sample was pretreated by He at 250 °C for an hour with 50 $ml \cdot min^{-1}$ which was controlled by a mass flow controller (Brooks, 5850E) and cooled down to room temperature.

1) CO adsorption

Each sample was treated for 24 h under CO oxidation condition. After the CO oxidation, the sample was cooled down to the room temperature under He atmosphere, and kept for an additional 30 min and background was collected. 10 % CO/He with 50 $ml \cdot min^{-1}$ of total flow was introduced for 30 min and He was purged for an additional 300 min to remove physisorbed CO. The DRIFTS spectra were obtained every 2 min from introducing CO gas using 128 scans with 4 cm^{-1} of resolution.

2) CO oxidation

Background spectrum was obtained at room temperature after He pretreatment at 250 °C for an hour. Then, 4 % CO, 10 % O_2, and 86 % He gases with 50 $ml \cdot min^{-1}$ of total flow rate were introduced into the reactor by MFC. The sample temperature was increased to 350 °C, and the DRIFTS spectra were collected every 5 °C with 128 scans and 4 cm^{-1} of resolution.

Density Functional Theory Calculations

We performed GGA-level spin-polarized density functional theory (DFT) calculations with the VASP code[8,9] and the PW91 functional[10]. The Ti *d*-orbitals and Ce *f*-orbitals were treated with the DFT+U method with U_{eff} = 4.5 eV applied for Ti and Ce ions[11]. The reliability of the U_{eff} value was experimentally verified by the XPS/UPS spectra of CeO_x supported on the rutile TiO_2 (110) system[12] and was confirmed in our previous study[13]. The interaction between the ionic core and the valence electrons was described by the projector augmented wave method[14], and the valence electrons were treated with a plane wave basis up to an energy cutoff of 400 eV. The Brillouin zone was sampled at the Γ-point. The convergence criteria for the electronic structure and the geometry were 10^{-4} eV and 0.03 $eV \cdot Å^{-1}$, respectively. We used the Gaussian smearing method with a finite temperature width of 0.05 eV improve convergence of states near the Fermi level.

A diagonal (surface vectors of [1 -1 -1] and [0 1 0]) 3×4 slab model with three layers of TiO_2 was used to model the TiO_2(101) surface. A CeO_2 cluster was deposited on TiO_2(101) to describe the morphology of the CeO_x-TiO_2 interface. Details of the thermodynamic interpretation of CeO_x-TiO_2 hybrid-oxide formation can be found elsewhere[12].

Microkinetic modeling of CO oxidation by Pt/CeO_2-TiO_2

The DFT-calculated rate map (turnover frequency, TOF) of CO oxidation by 0.05PCT (Pt_2/CeO_2-TiO_2) is estimated by the modified microkinetic modeling (ref. 29) based on the energetics presented in Fig. S4. The initial Pt_2/CeO_2-TiO_2 model with two pre-adsorbed CO molecules was used for modeling. Because the DFT-calculated binding energy, E_{bind}, of the first CO (-2.01 eV) and the second CO (-2.05 eV) is identical, we considered the sequential binding of two CO molecules as single event. Therefore, the surface concentration of the 2nd bound CO molecule can be estimated from the following reaction:

$2CO(g) + 2^* \rightarrow 2CO^*$ (R1: CO adsorption)

We used the average binding energy of two CO molecules for estimation of K1 (equilibrium constant). Because the R1 is in equilibrium, the rate can be written as:

$$rate(R1) = k_1^+ p(CO)\theta^* - k_1^- \theta^{CO} = 0$$

$$\theta^{CO} = \left(k_1^+ / k_1^-\right) p(CO)\theta^* = K_1 p(CO)\theta^*$$

where K_1 is the equilibrium constant for R1, $p(CO)$ represents the partial pressures of CO. k_1^+ and k_1^- is the forward and the backward rate constant of R1, respectively. The balance between the binding sites, θ^*, and the bound molecules (2COs), θ^{CO}, was calculated by assuming $\theta^{CO} + \theta^* = 1$. The equilibrium constants K_1 is,

$$K_1 = exp\left(\frac{-\Delta G_1}{kT}\right) = exp\left(\frac{-(\Delta E_{bind} - T\Delta S_{bind} + \Delta ZPE)}{kT}\right)$$

ΔE_{bind} : Average binding energy of 2 CO moleucles

ΔS_{bind} : Entropy change involved in CO adsorption

ΔZPE : Zero point energy change upon CO adsorption = 0.07 eV/molecule

The temperature dependent standard entropy of CO was adopted from the NIST

webbook (http://webbook.nist.gov). The O-C-O formation on Pt_2/CeO_2-TiO_2, which is the rate determining step of overall CO oxidation, requires an activation energy barrier of 0.75 eV (Fig. S2). Because the oxygen concentration dependency of the MvK mechanism of CO oxidation is low, the maximum reaction rate of O-C-O formation can be estimated as follow:

$$rate(O-C-O\ formation, the\ RDS) = \frac{kT}{h} exp\left(\frac{-(E_{act}^{+} - T\Delta S^{+})}{kT}\right)\theta^{CO}$$

E_{act}^{+} : Forward activation energy barrier

$\Delta S^{+} = 0$

2. Supplementary Figures and Tables

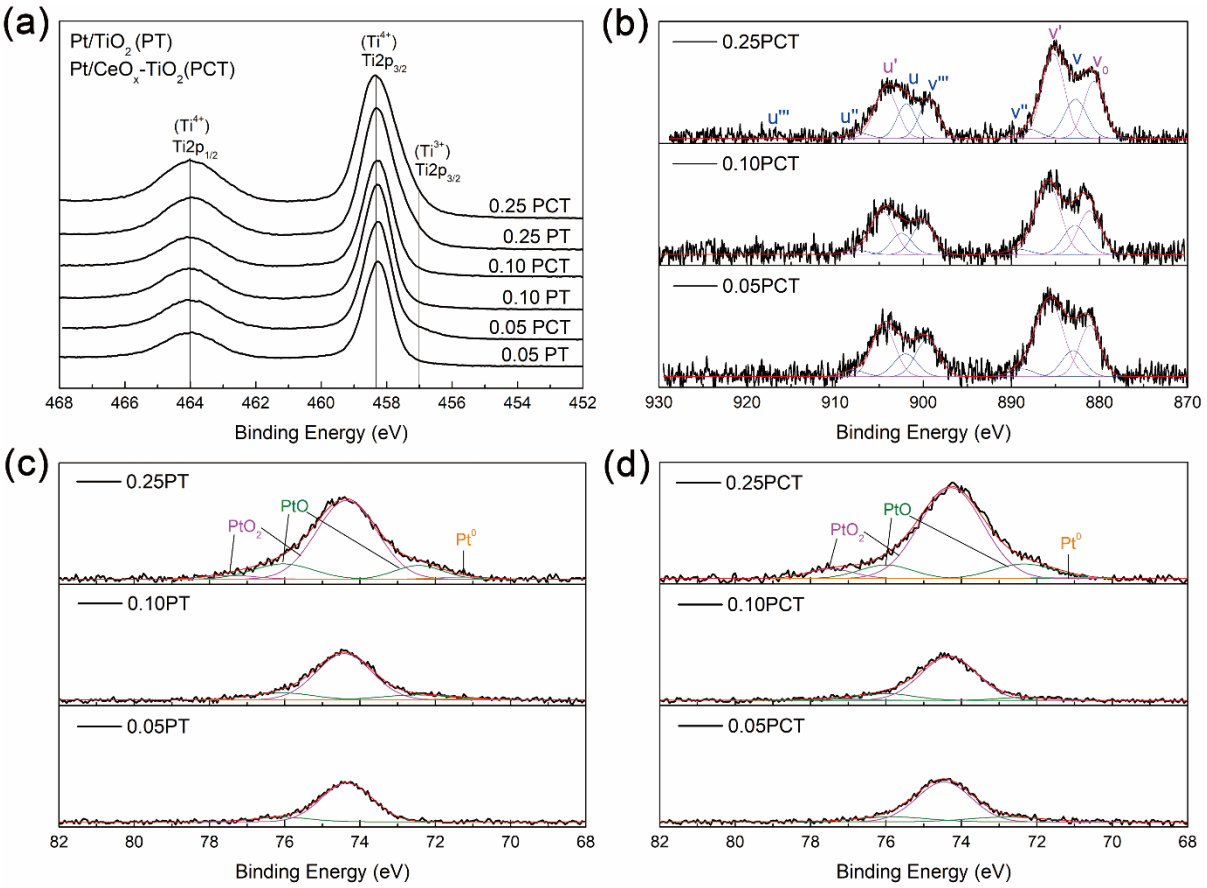

Figure S1. XPS spectra of *n*PT and *n*PCT. (**a**) Ti 2*p* spectra of *n*PT and *n*PCT. (**b**) Ce 3*d* spectra of *n*PCT. Refer to Table S1 for quantitative ratio of Ce^{3+} and Ce^{4+}. (**c** and **d**) Pt 4*f* spectra of *n*PT and *n*PCT catalysts. Refer to Table S1 for quantitative ratio of Pt^0, Pt^{2+}, and Pt^{4+}.

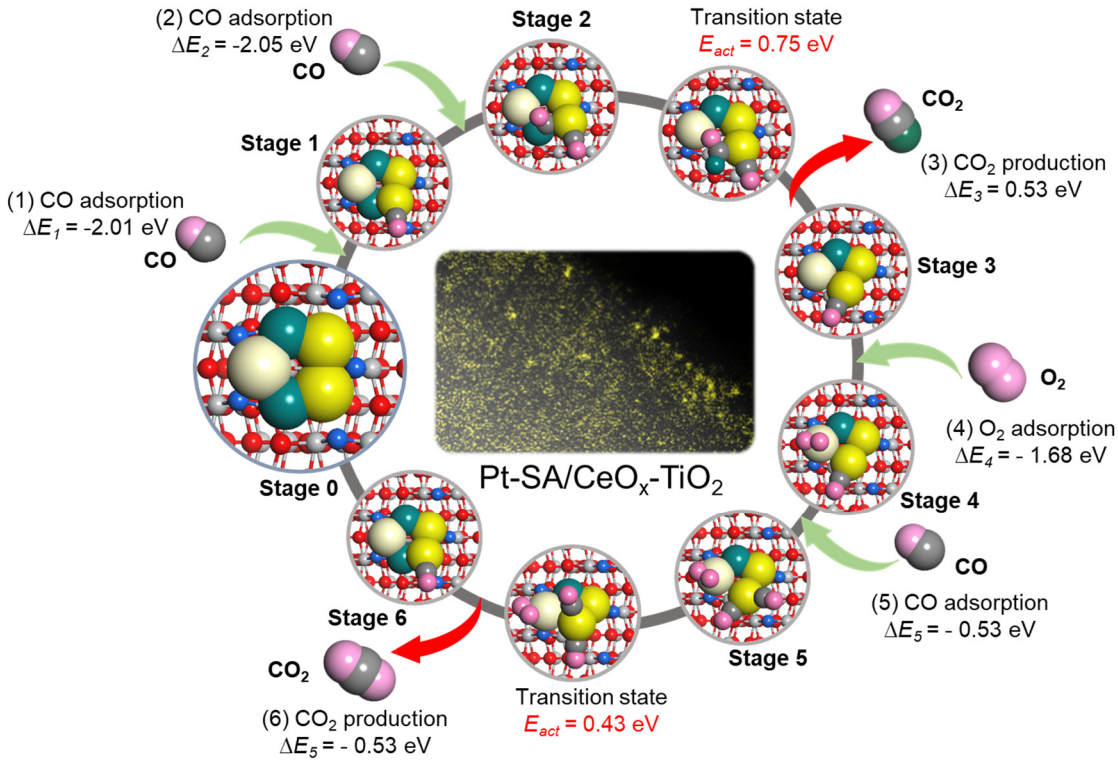

Figure S2. Schematic energetics and pathway of CO oxidation by Pt-SAs stabilized at CeO_x-TiO_2 interfaces through the Mars van-Krevelen mechanism. ΔE_n denotes the relative energy of the n^{th} stage with respect to the $(n\text{-}1)^{th}$ stage. For example, ΔE_3 was calculated as follows: ΔE_3 = Energy of stage 3 – Energy of stage 2. The original data was adopted from our previous report, *Energy Environ. Sci.* 2020, **13**, 1231-1239, by the permission of The Royal Society of Chemistry.

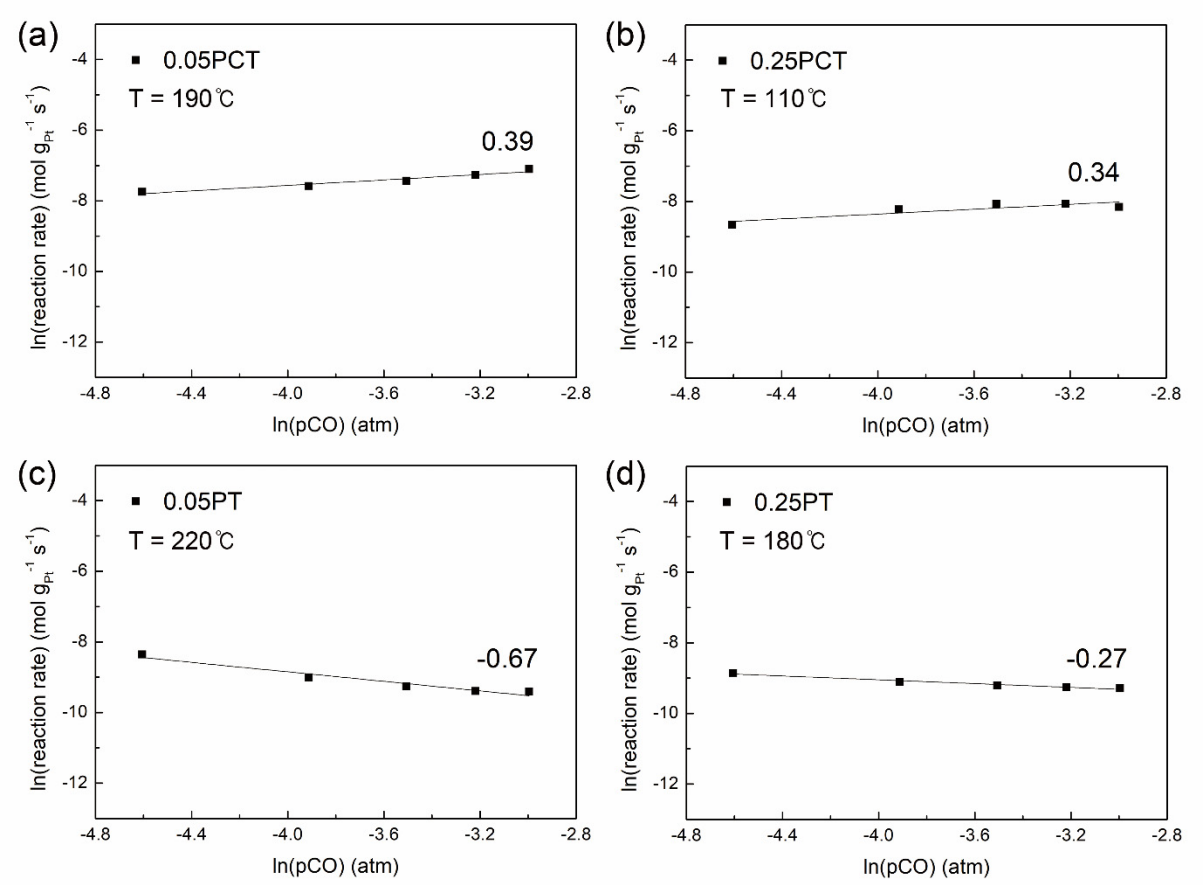

Figure S3. Order of reaction with CO. (**a**) 0.05PCT, (**b**) 0.25PCT, (**c**) 0.05PT, and (**d**) 0.25PT. Consistent positive order of reaction values with CO observed in 0.05PCT and 0.25PCT show that the nature of the reaction sites in these catalysts is identical and that the reaction sites are resistant to CO-poisoning. The highly negative order of reaction value with CO observed in 0.05PT confirms that the reaction centers in 0.05PT are CO-poisonable. The decreased, but still negative, order of reaction in 0.25PT shows that the CO-tolerance of the reaction sites in Pt/TiO_2 (*n*PT) catalysts is correlated with the size of Pt species.

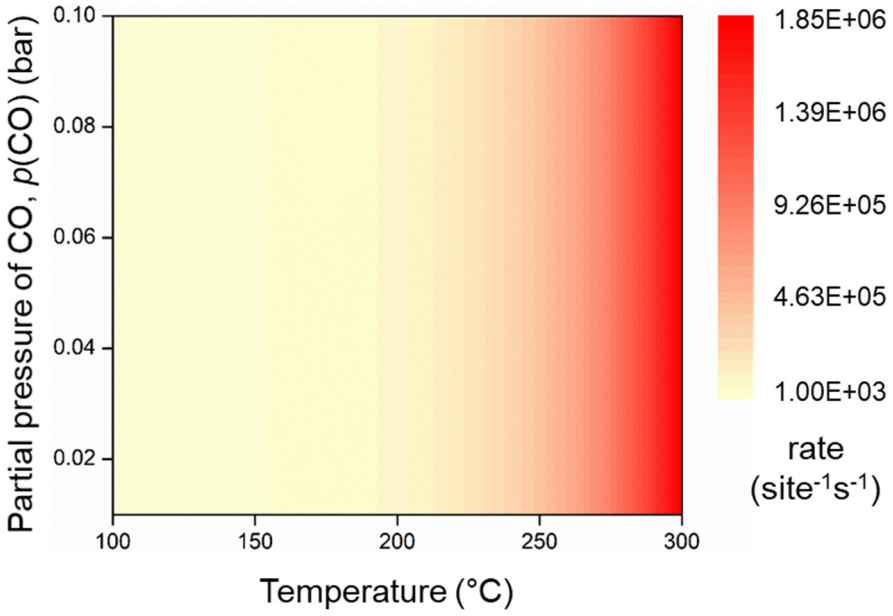

Figure S4. Specific reaction rate map of CO oxidation by 0.05PCT via the MvK mechanism (refer to Fig. S2 for energetics).

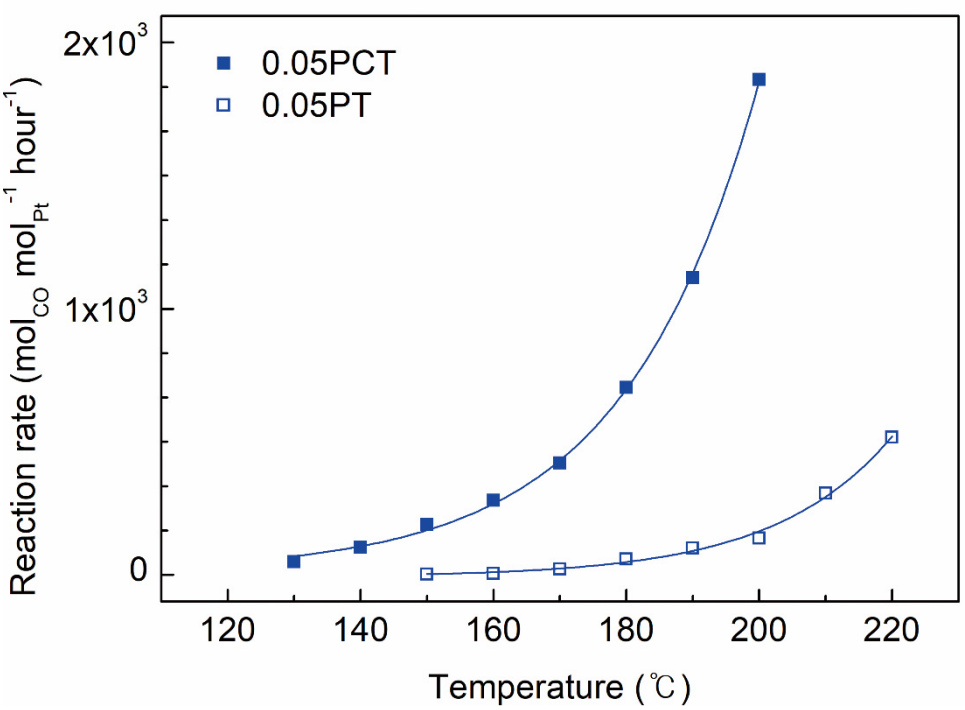

Figure S5. Temperature dependent specific activity of 0.05PT and 0.05PCT. The normalized specific reaction rate of 0.05PCT is 80 or 13.5 times greater than that of 0.05PT at 150 °C or 200 °C, respectively.

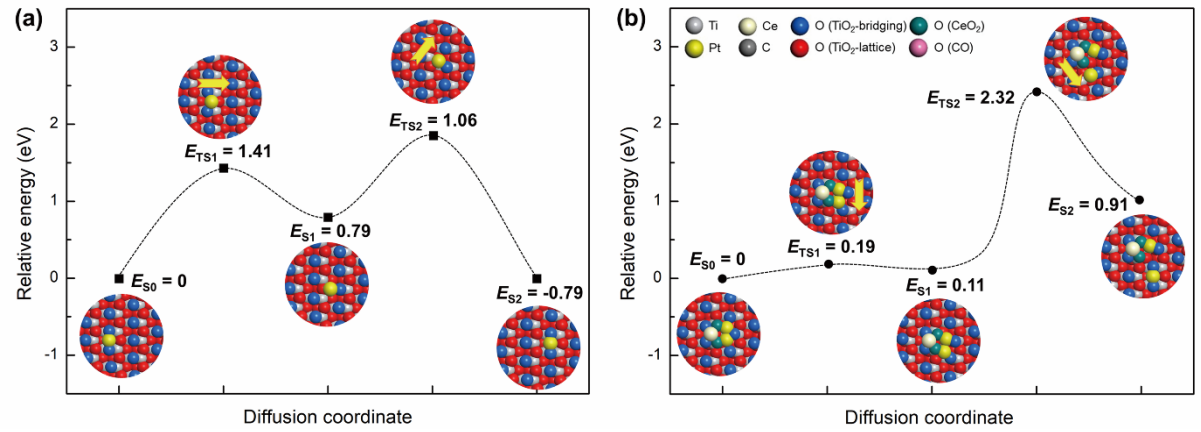

Figure S6. DFT-calculated diffusion energy barrier of Pt-SA. (**a**) on TiO_2(101) and (**b**) on CeO_x/TiO_2. The ΔE_{Sn} denotes the energy of the *n*-th state relative to the original state, *n*=0. The E_{TSn} represents the *n*-th transition state and the corresponding energy calculated with the climbing image-nudged elastic band methods. The reverse W shaped energy landscape presented in (**a**) confirms that a Pt-SA can be easily diffused out from the most stable binding site on the TiO_2(101) surface. The relatively higher barrier found in (**b**) (E_{TS2}) shows that a Pt-SA is anchored to the CeO_x-TiO_2 interface.

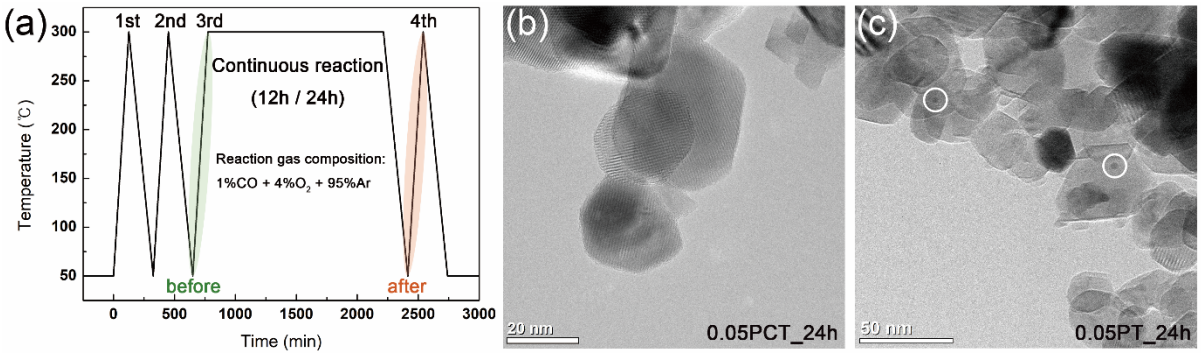

Figure S7. Long-term stability test. (**a**) Temperature profile for long-term reaction tests. STEM images of (**b**) 0.05PCT and (**c**) 0.05PT after 24 hours of high-temperature CO oxidation tests conducted at 300 °C. No significant agglomeration of Pt-SAs was observed in 0.05PCT, whereas large Pt-NPs were found in 0.05PT (white-circles).

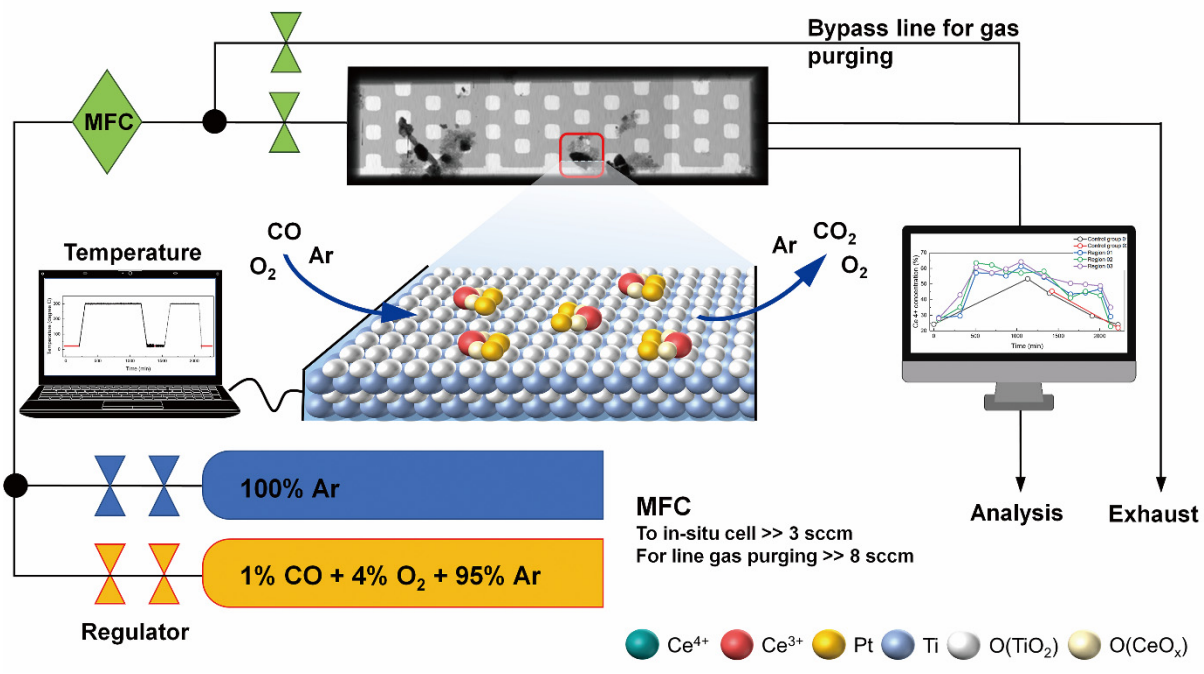

Figure S8. A schematic diagram of *operando* XAS/STXM analysis process.

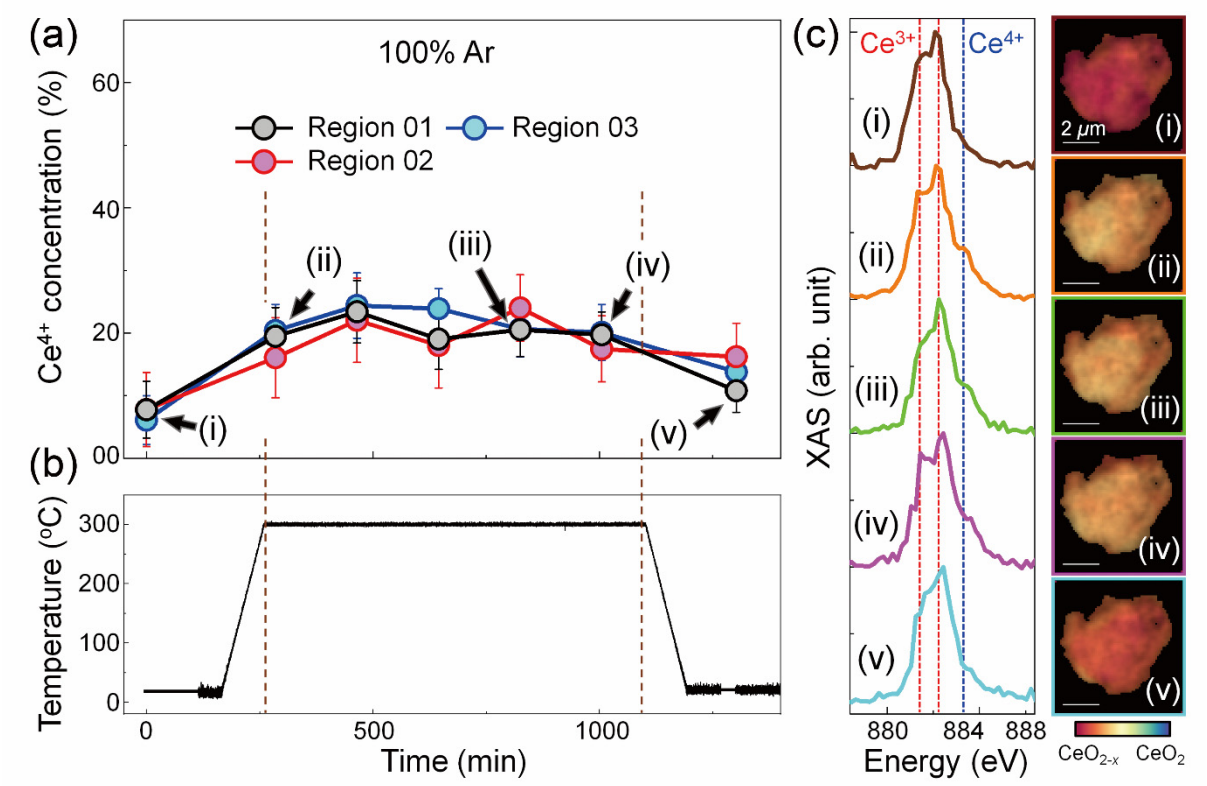

Figure S9. *Operando* gas XAS/STXM analysis result of 0.05PCT exposed to a stream of 100 vol.% Ar flow up to 300 °C. Averaged Ce^{4+} concentrations of 0.05PCT regions (**a**) with respect to the temperature profile (**b**). The error bars in (**a**) indicate the standard deviation. (**c**) *Operando* XAS from the region 1 (left) and their spatiotemporal chemical evolutions (right) specified in (**a**). Energy positions of M_5-edge absorption features for Ce^{3+} and Ce^{4+} are indicated as dotted red and blue lines, respectively. The fitting results (chemical information) and averaged optical density (morphological information) at each pixel were presented by color legend and transparency, respectively. The presence of CeO_2 and CeO_{2-x} assigned colors blue and red, respectively.

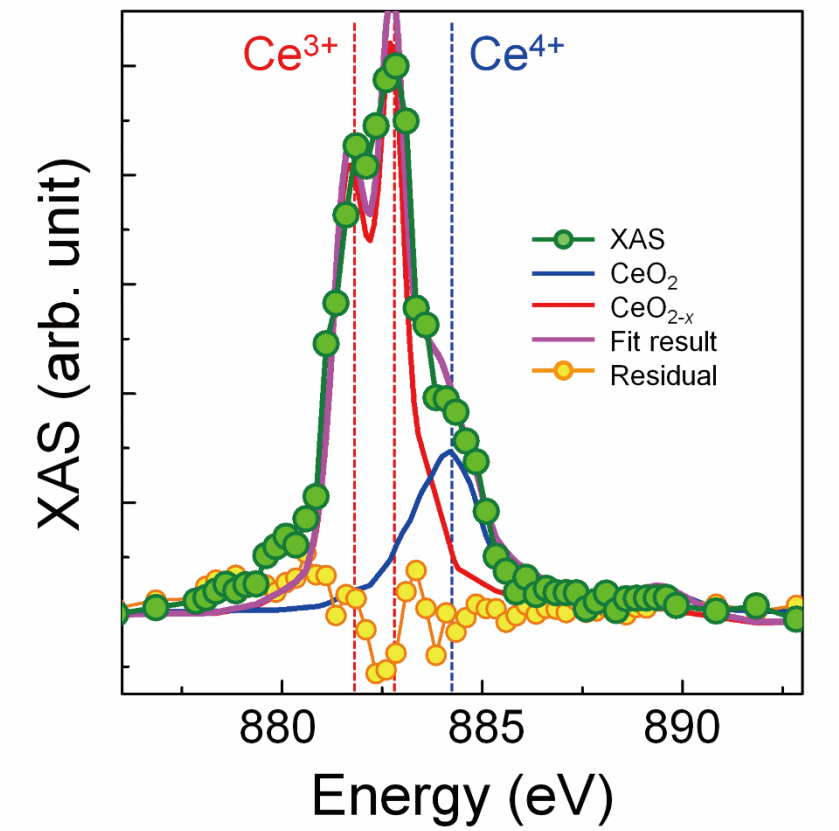

Figure S10. Quantitative determination of chemical composition by linear combination fits. Averaged Ce M_5-edge XAS of 0.05PCT (solid green line with filled circles). Simulated spectra (solid magenta line) is a result of a linear combination fit with reference spectra from CeO_x-TiO_2 with 1 wt.% Ce addition (CeO_{2-x}, solid red line) and pure CeO_2 (solid blue line)[1]. The residual spectrum (solid orange line with scatters) is the difference between the experimental and the simulated spectra. Energy positions of M_5-edge absorption features for Ce^{3+} and Ce^{4+} are indicated as dotted red and blue lines, respectively.

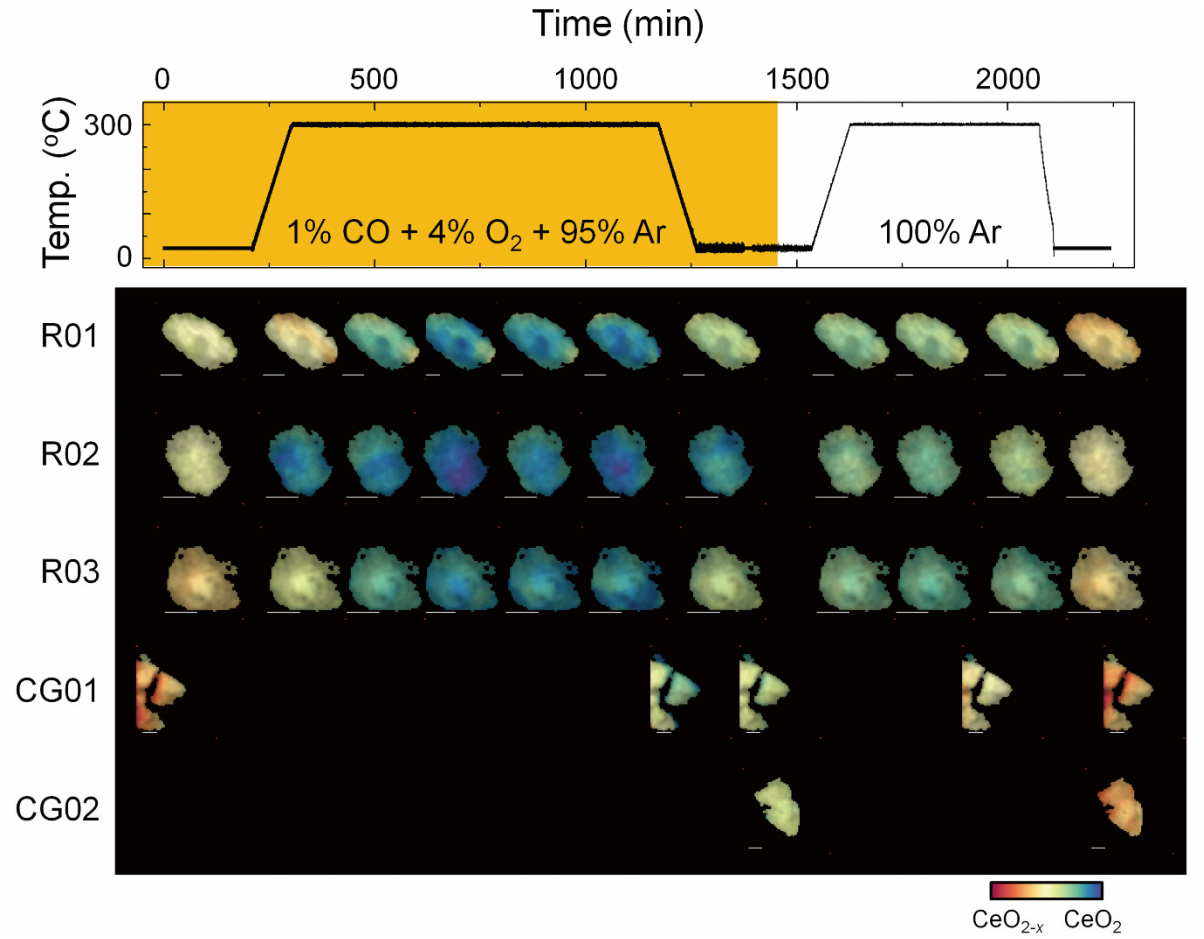

Figure S11. ***Operando*** **Ce chemical maps of 0.05PCT at elevated temperature (300 °C).** The types of gases with respect to the thermal-history are indicated as orange (1 vol.% CO + 4 vol.% O_2 + 95 vol.% Ar) and white (100 vol.% Ar) shaded areas. Spatiotemporal chemical evolutions of three experimental regions (R01, R02, and R03) and two control regions (CG01 and CG02) were obtained by linear combination fits of XAS data with reference spectra (Fig. S10). The fitting results (chemical information) and averaged optical density (morphological information) at each pixel were presented by color legend and transparency, respectively. The presence of CeO_2 and CeO_{2-x} assigned colors blue and red, respectively. All scale bars indicate 1 μm.

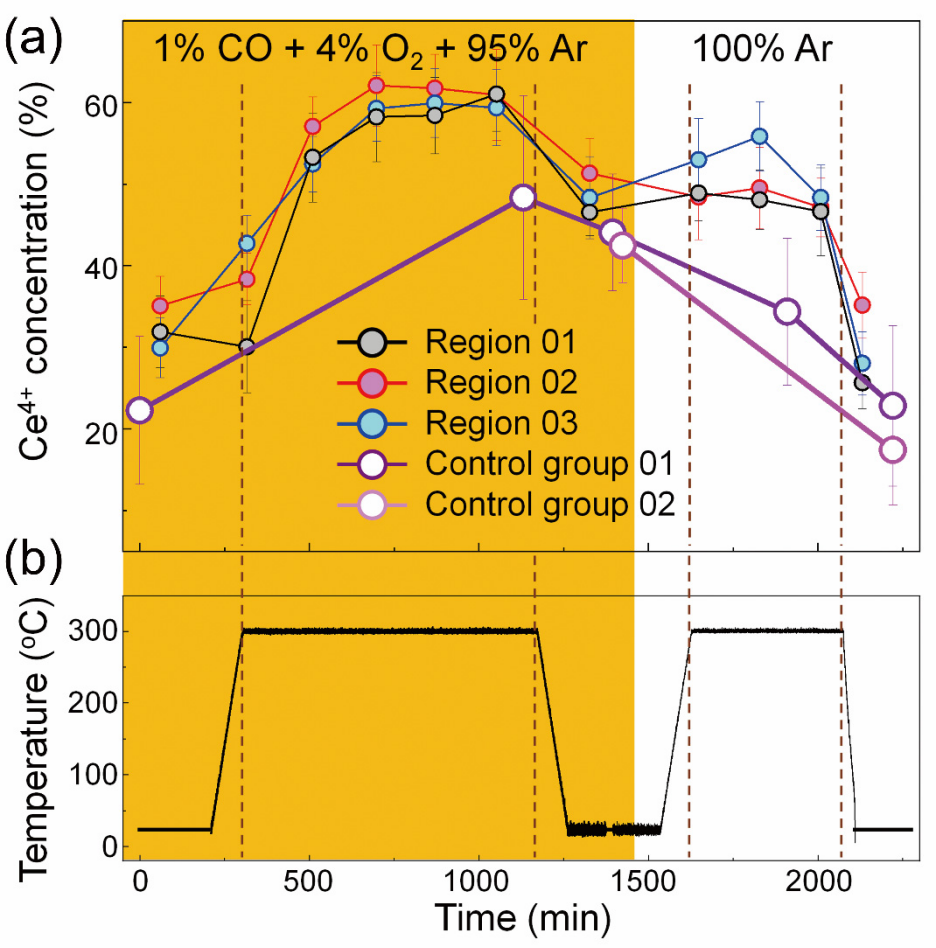

Figure S12. **Control groups for *operando* Ce chemical maps of 0.05PCT at elevated temperature (300°C).** (**a**) Overall Ce^{4+} concentrations of control groups and (**b**) temperature profile. Elevated temperature regions are clarified by dotted lines. The types of gases with respect to the thermal-history are indicated as orange (1 vol.% CO + 4 vol.% O_2 + 95 vol.% Ar) and white (100 vol.% Ar) shaded areas. For comparison, the results in Fig. 6c also are plotted (a).

Table S1. XPS analysis results of *n*PT and *n*PCT catalysts.

Catalysts	***n*PT**			***n*PCT**		
Pt-loading (wt.%)	**0.05**	**0.10**	**0.25**	**0.05**	**0.10**	**0.25**
Ce^{3+}	-	-	-	65.6	64.7	61.9
Ce^{4+}	-	-	-	34.4	35.3	38.1
PtO_x	100	98.68	98.42	100	100	99.03
Pt^0	**0**	**1.32**	**1.58**	**0**	**0**	**0.97**

Table S2. XANES linear fitting results of 0.05PT and 0.05PCT before and after long-term reaction test.

Catalyst	As-synthesized			After 24 hours		
	Pt	**PtO_2**	***R*-factor**	**Pt**	**PtO_2**	***R*-factor**
0.05PCT	0.8 %	99.2 %	5.15×10^{-4}	4.2 %	95.8 %	6.82×10^{-4}
0.05PT	7.5 %	92.5 %	5.77×10^{-4}	49.4 %	50.6 %	2.46×10^{-4}

Table S3. Summary of TOFs of CO oxidation of Pt-SAs available in literature.

Catalyst	Pt loading (wt.%)	Temperature (℃)	TOF×10^2 (s^{-1})	Activation energy (eV)	Reaction gas (vol.%)	Reference
Pt/CeO_x-TiO_2	0.05	190 (T_{20}) 202 (T_{50})	31.0 134.9	0.69	[CO] 1%, [O_2] 4%, balanced with Ar	This work
Pt/CeO_x-TiO_2	0.10	190 (T_{20}) 201 (T_{50})	23.7 127.6	0.68		
Pt/TiO_2	0.05	190 (T_{20})	2.8	1.22		
Pt/TiO_2	0.025	200	11.0	0.71	[CO] 1%, [O_2] 1%, balanced with He	*J. Am. Chem. Soc*., **139**, 14150–14165 (2017)
Pt/CeO_2	3.0	180 (T_{20})	7.2	NA	[CO] 1.9%, [O_2] 1.3%, balanced with He	*ACS Catal*., **9**, 3978-3990 (2019)
Pt/CeO_2-AT	1.0	80	0.5	0.55	[CO] 1.9%, [O_2] 1.3%, balanced with He	*Nat. Commun*., **10**, 1358 (2019)
Pt/CeO_2-SEA	1.0	80	1.3	0.50		
Pt/CeO_2	1.0	225 (T_{15})	17.0	0.57	[CO] 1.9%, [O_2] 1.3%, balanced with He	*Science*, **353**, 150–154 (2016)
Pt/Al_2O_3+CeO_2	1.1	225 (T_{15})	15.0	0.58		
Pt/CeO_2	1.0	250	1.0	1.09	[CO] 0.4%, [O_2] 10%, balanced with Ar	*Science*, **358**, 1419–1423 (2017)
Pt/CeO_2-steam	1.0	115	1.0	0.44		
Pt/CeO_2	0.27	150	1.7	0.89 (Exp.) 0.80 (The.)	[CO] 0.1%, [O_2] 5%, balanced with N_2	*Nat. Commun.,***10**, 3808 (2019)
Pt-O-Pt/CeO_2	0.27	150	197	0.41 (Exp.) 0.56 (The.)	[CO] 0.1%, [O_2] 5%, balanced with N_2	
Pt-O-Pt/CeO_2-wet	0.27	50	60	NA	[CO] 0.1%, [O_2] 5%, [H_2O] 3%,	

					balanced with N_2	
Pt/FeO_x	0.17	27(T_{15})	13.6	0.49	[CO] 1%, [O_2] 1%, balanced with He	*Nat. Chem*., **3**, 634-641 (2011)
Pt/FeO_x	0.17	80 (T_{20})	16.5	0.79	[CO] 1%, [O_2] 1%, [H_2] 40%, balanced with He	*J. Phys. Chem. C.*, **118**, 21945–21951 (2014)
Pt/Fe_2O_3	0.029	180	8.7	0.70	[CO] 1%, [O_2] 4%, balanced with He	*Ind. Eng. Chem. Res*., **56**, 6916–6925 (2017)
Pt/γ-Al_2O_3	0.044	180	7.7	0.95		
Pt/ZnO	0.034	180 (T_{50})	7.4	0.81		
Pt/meso-Al_2O_3	0.2	200 250 (T_{15})	2.3 17.5	0.83	[CO] 2.5%, [O_2] 2.5%, balanced with Ar	*Nat. Commun*., **8**, 16100 (2017)
Pt/θ-Al_2O_3	0.18	251 (T_{20})	18.7	NA	[CO] 3.7%, [O_2] 3.7%, balanced with He	*J. Am. Chem. Soc.*, **135**, 12634-12645 (2013)
Pt/CeO_2-Al_2O_3	1.0	106 (T_{30})	14.5	NA	[CO] 1%, [O_2] 1%, balanced with He	*Angew. Chem. Int. Ed.*, **56**, 20691-20696 (2020)

3. References

1. M. Yoo, Y.-S. Yu, H. Ha, S. Lee, J.-S. Choi, S. Oh, E. Kang, H. Choi, H. An, K.-S. Lee, J. Y. Park, R. Celestre, M. A. Marcus, K. Nowrouzi, D. Taube, D. A. Shapiro, W. Jung, C. Kim and H. Y. Kim, *Energy & Environmental Science*, 2020, **13**, 1231-1239.
2. J. F. Moulder and J. Chastain, *Handbook of x-ray photoelectron spectroscopy : a reference book of standard spectra for identification and interpretation of XPS data*, Physical Electronics Division, Perkin-Elmer Corp., Eden Prairie, Minn., 1992.
3. *Journal*, 2020, DOI: 10.18434/T4T88K.
4. S. M. Webb, *Phys Scripta*, 2005, **2005**, 1011-1014.
5. D. A. Shapiro, R. Celestre, B. Enders, J. Joseph, H. Krishnan, M. A. Marcus, K. Nowrouzi, H. Padmore, J. Park, A. Warwick and Y.-S. Yu, *Microscopy and Microanalysis*, 2018, **24**, 8-11.
6. H. L. Xin, K. Niu, D. H. Alsem and H. Zheng, *Microscopy and Microanalysis*, 2013, **19**, 1558-1568.
7. Y. A. Wu, L. Li, Z. Li, A. Kinaci, M. K. Y. Chan, Y. Sun, J. R. Guest, I. McNulty, T. Rajh and Y. Liu, *ACS Nano*, 2016, **10**, 3738-3746.
8. G. Kresse and J. Furthmuller, *Phys Rev B*, 1996, **54**, 11169-11186.
9. G. Kresse and D. Joubert, *Phys Rev B*, 1999, **59**, 1758-1775.
10. J. P. Perdew and Y. Wang, *Phys Rev B*, 1992, **45**, 13244-13249.
11. S. L. Dudarev, G. A. Botton, S. Y. Savrasov, C. J. Humphreys and A. P. Sutton, *Phys Rev B*, 1998, **57**, 1505-1509.
12. J. B. Park, J. Graciani, J. Evans, D. Stacchiola, S. G. Ma, P. Liu, A. Nambu, J. F. Sanz, J. Hrbek and J. A. Rodriguez, *P Natl Acad Sci USA*, 2009, **106**, 4975-4980.
13. H. Y. Kim, M. S. Hybertsen and P. Liu, *Nano Letters*, 2017, **17**, 348-354.
14. P. E. Blochl, *Phys Rev B*, 1994, **50**, 17953-17979.